INSPIRE

IN-situ Sampling and Primal Investigation Rover on Europa

Phase 0/A-Study of a Rover Mission on the Surface of the Jupiter moon Europa

Denis Acker
Daniel Bölke
Korbinian Kasper
Christian Korn
Nicolas Probst
Saskia Sütterlin

Supervisors:
Moritz Nitz M.Sc.
Patrick Winterhalder M.Sc.

Symbols

Symbol	Definition	Unit
a	Constant for the Geometry of a Porous Media	nm
A	Wheel Ground Contact Area	m
b	Wheel Width	m
c	Coefficient of Soil Cohesion	Pa
$C_{\text{Batt,req}}$	Total Required Battery Capacity	Wh
$C_{\text{Batt,req}}$	Battery Nominal Capacity	Wh
C_{cell}	Cell Voltage	V
C_{rr}	Rolling Resistance Coefficient	-
d	Wheel Diameter	m
DoD	Depth of Discharge	%
DP	Drawbar Pull	N
H	Soil Thrust	N
h_{Ice}	Ice Crust Surface Thickness on Europa	m
k_{c}	Sinkage Modulus	$\frac{\text{kN}}{\text{m}^{n+2}}$
k_{ϕ}	Soil Friction Angle Sinkage Modulus	$\frac{\text{kN}}{\text{m}^{n+3}}$
l	Ground Contact Length	m
T_{Surface}	Surface Temperature on Europa	K
M	Number of Cells in Parallel	-
m_{RTG}	RTG Mass	kg
m_{w}	Weight per Wheel	kg
n	Soil Deformation Exponent	-
N	Number of Cells in Series	-
P_{el}	RTG Electrical Power	W_{el}
$P_{\text{el,req}}$	Required Electrical Power	W_{el}
P_{mode}	Demanded Electrical Power per Mode	W_{el}
R_{b}	Bulldozing Resistance	N
R_{c}	Compaction Resistance	N
R_{g}	Gravitational Resistance	N
R_{r}	Rolling Resistance	N
t_{e}	Mode Duration	s
W_{wheel}	Normal Force per Wheel	N
z	Sinkage	m
α_{BOL}	BOL Specific Power	$\frac{W_{el}}{kg}$
ϵ	Emissivity	-
η_{LiIon}	Efficiency of LiIon Cells	-
ϕ	Friciton Angle	°
ρ_{Ice}	Inner Encoder Ring Diameter	$\frac{\text{kg}}{m^3}$

θ Slope Angle $^\circ$

Abbreviations

BOL	Begin of Life
BOM	Begin of Mission
COMM	Communications
C&DH	Command & Data Handling
CPU	Core Processing Unit
DoD	Depth of Discharge
EOM	End of Mission
EPS	Electrical Power System
FEC	Forward Error Correction
HGA	High Gain Antenna
LGA	Low Gain Antenna
2D	Two Dimensional
3D	Three Dimensional
PCDU	Power Control and Distribution Unit
PCU	Power Control Unit
PDU	Power Distribution and Control Unit
IMU	Inertial Measurement Unit
IRS	Institute of space Systems at the University of Stuttgart
INSPIRE	IN-situ Sampling and Primal Investigation Rover on Europa
ESA	European Space Agency
MMP	Mean Maximum Pressure
NASA	National Aeronautics and Space Administration
SPENVIS	SPace ENVironment Information System
HPC	High Priority Commands
RTG	Radioisotope Thermoelectric Generator
eMMRTG	Enhanced Multi Mission Radioisotope Thermoelectric Generator
eSMMRTG	Enhanced and Scaled Multi Mission Radioisotope Thermoelectric Generator (3kg)
TID	Total Ionizing Dose
OBC	On-Board Computer
S/C	
SBC	Single Board Computer

Contents

List of Figures

List of Tables

Chapter 1

The Mission

During the observation of Jupiter, the Glileo spacecraft did also some flybys of the Jupiter moons, [1]. The scientist gahtered data from Europa, which suported the evidence of a thick icy surface. The possibility of liquid water underneath lead astrobiologists to the assumption that extraterrestrial life could exist on Europa, [2]. That is why Europo is - beside Mars - an interesting object of research.

Therefore, the ESA will launch the *JUICE* oriber in 2022 to investigate Europa in more detail, [3]. But also the NASA is developing *Europa Clipper* to get detailed information. Additionally, they plan a lander for Europer to bring scientific instruments onto the surface. [4] [5].
Under the leadership of Prof. Dr.-Ing. Klinkner, the Institute of Aero Space Systems started within a seminar a feasibility study about a rover system to explore Europa surface, which shall be part of the *TRIPLE* mission. This challenge was given to five student teams in order to develop concepts, construct preliminary designs, perform analysis and make evaluations to meet the mission objectives and fit the mandatory requirements cite.

This report contain the results of the Phase A study of the rover system IN-situ Sampling and Primal Investigation Rover on Europa (INSPIRE).

Chapter 2

Payload

2.1 Sterovision Camera / Observation / Perception

The INSPIRE rover is equipped with five individual cameras. Two are used as stereo vision cameras on an hight adjustable and rotatable telescope arm on the front side of the rover. This ist used to capture a detailed 3D model of the environment with which sizes and distances can be estimated. The remaining three cameras are used as has-cameras which are necessary to obtain data regarding the nearby environment. All cameras are equipped with radiation hardened lenses to prevent browning of the lenses. The main tasks of the camera system is the provision of scientific data and navigation related data. More details regarding the navigation and autonomy are provided in Section 4.8.

2.2 Ground RADAR

2.3 Ice Core Drill

2.4 RadHard Solar Arrays

As a secondary mission goal for INSPIRE a cooperation with the european project RadHard which is led by the german solar array manufacturer Azure Space is intended. They are currently developing a new generation of 4 Junction solar cells with an efficiency of up to 35%. But the main feature of the new solar arrays is their radiation hardness which will be the highest radiation hardness ever designed with an efficiency of $> 3\%$ after $1E15 \ cm^{-2} \ 1MeV$ electron irradiation. So the Jupiter environment with its extreme radiation would be the best suitable destination for a test and evaulation mission of this new technology. Therefore INSPIRE will be equipped with 8 RadHard solar cells with a total surface area of $0.0248m^2$ for a technology demonstration[6].

Chapter 3

Operation

.....

3.1 Mission Phases

For the INSPIRE Mission Phase 0 study five basic mission phases have been defined. Furthermore a sixed optional mission phase after the nominal mission lifetime has been established which will be conducted if the rover is still operational after its nominal lifetime.

- **Phase 0:** Launch and Flight Phase
- **Phase 1:** Entry, Descent and Landing Phase
- **Phase 2:** Depolyment Phase
- **Phase 3:** Egress, Comissioning and Early Operation Phase
- **Phase 4:** Mission Operation Phase
- (**Phase 5:** Exceeding Mission Operation Phase)
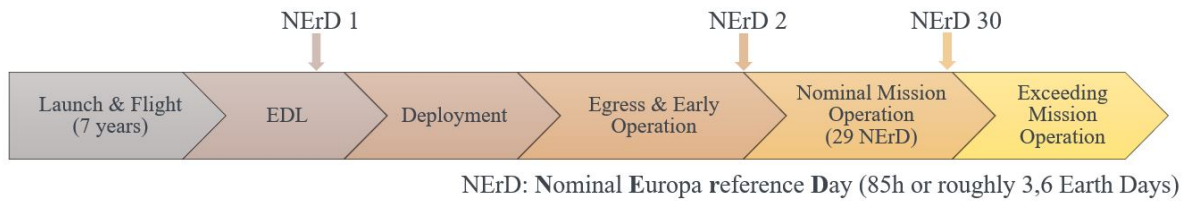
Figure 3.1: Preliminary Mission Timeline for INSPIRE.

Based on these missions phases some preliminary rover system modes as well as a basic mission timeline were concluded.

3.1.1 Rover System Modes

For this case study several rover system modes were defined. All ten modes are listed in Table 3.1. They are seperated into two groups. The design critical modes are displayed in white and are defined as system modes, which significantly influence the preliminary design of the rover subsystem like the thermal or power subsystem. None design critical modes (grey) also have a major influence on multiple subsystems of the rover but play a secondary role in the thermal and power budget of the rover for this Phase 0 study. These non design critical modes extend from the rover storage and launch until the finale deployment of the rover is completed. These modes and their design options depend heavily on the final design of the lander with which INSPIRE flies to Europe. Therefore, a clear definition of such modes is not possible at this time in the course of this phase 0 study. However, the respective considerations, preferences and options have been briefly described in the mode descriptions. It is important to note that INSPIRE's

goal is to provide a flexible rover design with as few hard requirements as possible for the parent lander. Therefore, many aspects of the rover, as well as the none design critical modes, will need to be further defined and elaborated in later phases of the project in close consultation with the customer.

For example, the exact interfaces between rover and lander should be defined in more detail. Depending on the subsequently chosen interfaces, many possibilities may arise in the corresponding rover system modes. With an appropriate interface, for example, the excess electrical and thermal energy of the RTG, which is already active during the flight, could be used to supply the lander system with heat and power. A corresponding interface could also enable the transmission of health checks from INSPIRE.

The deployment phase will strongly depend on the final design of the lander, INSPIRE's position within the lander and also the possibilities that the lander provides to INSPIRE. Possible deployment strategies would be as follows:

- **Option 1:** If INSPIRE on ground level: Release from storage box through spring mechanism or actuators. Rover storage configuration allows rolling and possible motorized actuation

- **Option 2:** If INSPIRE is above ground level: Similar as Option 1 but an additonal ramp and ramp deployment would be required.

- **Option 3:** INSPIRE will be deployed through the landers robotic arm if it is capable of lifting its mass.

Number	Rover System Modes	Abbreration	Definition
0	Launch/Off Mode	OFF	From Launch until EDL Phase Rover System is OFF Exact mode description t.b.d. and can be adapted to meet the lander demands Health tests on Occasion during flight time are foreseen (PCDU could be active) Batteries on Storage Capacity at launch and may be recharged on occasion (like Rosetta Mission) Telemetry data shall be sent by the Lander (optional if possible) RTG on =>Electrical and Thermal Power may be used (for Lander Power and Thermal Systems) or is disposed of by shunts
1	Entry, Descent and Landing	EDL	From Entry until next morning after secure landing of Lander on Europa See Mode OFF PCDU ON after secure landing (Powered by RTG) Heaters ON (powered by remaining RTG Power) Battery charging if no Kill Switch is used
2	Deployment and Early Operation Mode	EOP	First Morning after EDL Exact mode description t.b.d. and can be customized to lander =>Dependant on final Lander Design Critical Deployments (Egress System) and leaving the lander Optional whether Kill Switch ejected =>Battery charging can start Rover System Activation possibilities: Kill Switch, Lander Interface, HPC from Earth PCDU ON OBC ON Heaters ON After sufficient Battery Capacity is reached (50%): Deployment of Rover Boogie and checkout/health check of all Rover Systems Afterward switching to Charging Mode
3	Idle/ Perception	ID	During Idle Operation Time Rover powered by RTG or Batteries (Excess Power charges Batteries) PCDU ON All Components in Standby or Power Saving Mode if possible Stereovision Camera ON for Orientation and Observation (Science Data) Hazcams and OBC ON for Orientation and Path Analysation COMM ON for larger time intervals (Listening Mode)
4	Safe Mode/ Hibernation (SAFE)	SAFE	Entered in case of emergency or contingency Rover Survival Mode =>Minimum Power PCDU ON COMM sends Emergency Signal then switches to COMM ON for small time intervals (Listening Mode) OBC OFF until Command received =>High Power Commands (HPC) Heaters ON Science data shall be stored without data loss Applicable during Day and Nighttime Exit after receiving the corresponding command (Optional: Timer ON and Restart of Rover System after time period has passed)
6	Communication	COMM	During Transmission of major Telemetry or Science Data Rover powered by RTG or Batteries (Excess Power charges Batteries) PCDU ON All Components in Standby or Power Saving Mode if possible OBC SB COMM ON (Transmission Mode)
7	Charging	BAT	For Battery charging Rover batteries charged by RTG PCDU ON All Components in Standby or Power Saving Mode if possible OBC SB Quit after sufficient charge is reached
8	Locomotion	LOC	For Rover Movement and Observation Locomotion and Navigation ON Hazcams and Traversing Path Analysis ON OBC ON PCDU ON COMM OFF Stereovision Camera ON for Orientation and Observation (Science Data) Only during Daytime
9	Payload Observation Mode	OBS	Payload Mode for Science Data Collection during Daytime OBC ON PCDU ON COMM OFF Stereovision Camera ON for Orientation and Observation (Science Data) RADAR ON for Ground Investigation =>Drill Location Only during Daytime
10	Payload: Ice Core Mode	ICE	Payload Mode for Science Data Collection during Daytime or Nighttime OBC ON PCDU ON COMM OFF Ice Core Drill ON during Ice Core Sample Collection Afterwards Sample will be analysed =>APXS ON

Table 3.1: Collection of Rover System Modes. [Kommt noch in Anhang]

Chapter 4

Subsystems

.....

4.1 Rover

...

4.2 Structure and Mechanics

...

4.3 Communications and Command and Data-Handling

The Communications and C&DH subsystem is responsible for the execution of Telecommand and Telemetry as well as payload data storing and transmission. Therefore the system consists of a pair of redundant Transmitter and Receiver as well as a redundant Single Board Computer OBC. The subsystem is located within the Electronic Bay.

4.3.1 Communication System

Requiring too many resources a direct link to earth has been deemed impractical. Instead communication for the INSPIRE mission is proposed to rely on a link between the rover and the Europa Lander. The lander then forwards data to earth via a satellite relay carrier which orbits the moon. The lander offers a 25 dB high gain antenna [Missing Reference] and a low gain antenna which is not further specified in literature.

The downlink from the rover to the lander has been identified as the critical transmission path. However, link budget considerations reveal that a transmission to the LGA of the Europa Lander produces a link margin of 15.14 dB, resulting in a Bit Error Rate of less than 10^{-6}.

Using the Landers LGA greatly increases robustness due to the elimination of pointing errors and higher margin for rover positioning error. Additionally, the INSPIRE rover's communication link would not interfere with the Landers communication to the relay carrier by blocking the HGA. The link budget has been performed under the conservative considerations listed in Table [Missing Reference]. The complete link budget can be found in Appendix [Missing Reference].

Component Selection

Due to the considerably high link margin the focus is on low mass and low power components with flight heritage such as flown on CubeSat missions. Criteria with relatively small impact on the link budget such as component noise or even FEC have not been taken into account. Ideally the rover communication uses X-Band for increased compatibility with the lander and has a total system mass of less than 1 kg.

Since radiation hardness was not included in most datasheets a total dose of < 20 $krad$ was assumed in accordance with values for LEO [Missing Reference].

Transmitter

Since the transmission duty cycle is short, mass has become the design driving criteria followed by power. Output power is found sufficient in the dBm regime. Subsequently the Transmitter Sputnix SXC-XTX-01 is selected for its low mass at 0.195 kg and high data rate of up to 10 $Mbps$ [Missing Reference].

Receiver

Acting as the life line connection to mission control the receiver is required to run high duty cycles. Thus, low power consumption has become the design driving criteria followed by mass. Ultimately the Endurosat S-Band receiver is chosen due to its exceptional low power consumption of 2 W and low mass of 0.220 kg [Missing Reference]. However, as a S-Band receiver the device would have to be adapted which means an increase in rover design complexity.

Antenna

A set of four omnidirectional low gain antennas is positioned on the rover chassis to produce a half sphere coverage around the rover. Due to the high frequency, the antenna can be compact while remaining a passive component to save power. With mass being the dominating factor in the trade off the Endurosat X-Band single patch antenna with a mass of 2.2 g seems fit [Missing Reference].

4.3.2 Command & Data Handling

With respect to restricted power supply a redundant OBC hot-cold configuration stands to reason. Additionally, the standby mode is suggested during hibernation and charging modes relying solely on the PCDU (see chapter [Missing Reference]). Emphasis for the Electronics selection is placed on flight proven radiation hardness to increase mission robustness in the high radiation environment of the Jupiter system. Criteria of less importance are CPU speed and dimensions.

Instead of designing a new OBC board a trade-off was performed among existing single board computers. SBCs provide peripheral services such as bus interfaces, timer and memory in a flight proven configuration, which promises a simplified mission development.

BAE Systems provides a SBC with their flight proven Power PC750 Architecture which withstands a total radiation dose of up to 1 $Mrad$. The robustness comes at the cost of a 182 MHz processor speed.

Additionally a custom housekeeping board will be tasked with providing engine control peripherals and sensor read out electronics.

4.4 Payload

...

4.5 Electrical Power System

The EPS (Electrical Power System) is the subsystem responsible for the electrical power supply of INSPIRE. It consists of four funadmental parts, which are the energy source, the PCDU unit

(Power Control and Distribution)and the Energy Storage as well as the rover subsystems as the consumers. The EPS is visualized in Figure 4.1.
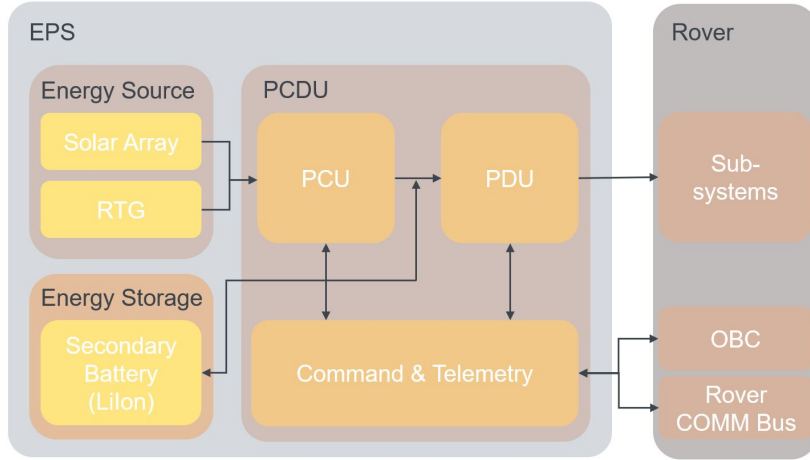
Figure 4.1: Functional Flow Chart Diagram for the EPS Subsystem.

4.5.1 EPS Budget and Overview

Table 4.1 summarizes the power budget of INSPIRE based on the rover system modes defined in Subsection 3.1.1. The complete power budget can be found in Figure A.1. As can be seen, the Locomotion mode has the highest demands on the EPS. Communication mode also has a high consumption. However, since this is primarily used at night and the rover can be charged again afterwards without any problems, it does not place any major restrictions on the power budget. Idle/Perception mode has a low consumption, but is usually used for a long time at a stretch and therefore also places high demands on the EPS. In Charging mode, the EPS is able to charge 7.04 W_{el}.

Rover System Mode	Total Rover Power Demand including battery charge $P_{\mathbf{mode}}$ [W_{el}]
Idle/Perception	15.25
Safe/Hibernation	−5.84
Communication	36.92
Charging	−7.04
Locomotion	232.36
Payload: Observation	15.41
Payload: Ice Core Mode	9.77

Table 4.1: Overview of the Power Budget of INSPIRE.

4.5.2 Energy Source

For the energy generation of INSPIRE many possible sources were taken into consideration for a trade-off. As a conclusion of this trad-off the decision was made to utilize a Radioisotope Thermoelectric Generator (RTG) as the main energy source for INSPIRE.

As the research couldn't find an RTG with a mass suitable for INSPIRE, the solution was to scale down a bigger RTG as an approximation. As a baseline of the scaling the eMMRTG (Enhanced Multi Mission Radioisotope Thermoelectric Generator) was utilized, which is currently under development at NASA and is especially designed for deep space missions like Europa. For the scaling a goal RTG mass of $m_{\text{RTG}} = 3$ kg was defined and the eMMRTG was scaled down using the given data.

In Table 4.2 the scaling results for the eSMMRTG (Enhanced and Scaled Multi Mission Radioisotope Thermoelectric Generator) are listed. The eSMMRTG has a BOL specific power of $\alpha_{\text{BOL}} = 4.0 \; \frac{W_{el}}{kg}$ and provides an electrical power of $P_{el} = 12.08 \; W_{el}$ during the mission duration[7][8][9][10][11].

Scaled eSMMRTG Parameter	
System Mass m_{RTG} [kg]	**3.5**
BOL Specific Power α_{BOL} $\frac{W_{el}}{kg}$	4.0
BOL Power $P_{el,\text{BOL}}$ W_{el}	14
Isotrop	Pu-238
Isotrop Half-Life [a]	87.7
Flight time and Storage (incl. Margins) [a]	7
Power Loss Degradation until BOM W_{el}	0.56
BOM Power $P_{el,\text{BOM}}$ W_{el}	13.44
Europa Day Duration [h]	85
Mission Duration [d]	106.25
End of Mission Power $P_{el,\text{EOM}}$ [W_{el}]	13.42
Final Power for Study P_{el} [W_{el}] (incl. 10% scaling Margin)	**12.08**

Table 4.2: Parameters for the scaled eSMMRTG based on the eMMRTG.

Furthermore INSPIRE will also be equipped with some radiation hardend solar arrays as already explained in Section 2.4[6]. Since these solar cells are primarily used for technology testing, the mission must also be able to operate completely without this generated energy. For this reason, and because the expected energy generated by the solar cells is minimal, only the energy generated by the RTG is considered for the Phase 0 Study. However, it should be noted that these solar cells will also generate a certain amount of energy, which will benefitial for the EPS.

4.5.3 Energy Storage

For the energy storage of INSPIRE many possible battery types were taken into consideration for a trade-off. As a conclusion of this trad-off the decision was made to utilize LiIon batteries as the secondary batteries of INSPIRE. This decision is primarily based on LiIon batteries high energy density, temperature range, robust performance and long operating and cycle life in extreme environments[12].

As the RTG only generates a small constant power the main energy source during the mission will be the accumulated energy of the batteries. The rover will charge the batteries at night, so the next exploration day can start with full capacity. Furthermore the batteries have to be charged during day time to maintain operations.

For the sizing of the batteries, the rover motion was chosen as the design driver, since this is the highest energy consuming state of the rover and additionally mission critical for INSPIRE. The rover motion consists of an interaction of the Locomotion and Perception mode as already

mentioned in Chapter 3. Therefore it was defined that INSPIRE shall be able to drive 50 m (including alternating Locomotion and Perception Mode) with a fully charged Battery. The required battery capacity $C_{\text{Batt,req}}$ can be caculated using Equation 4.1. The results are listed in Table 4.3 [13].

$$C_{\text{Batt,req}} = \frac{P_{\text{el,req}} \cdot t_e}{DoD \cdot \eta_{\text{LiIon}}} \quad (4.1)$$

Power Consumption Mode:	Locomotion	Perception
Required Electrical Power $P_{\text{el,req}}$ $[W_{el}]$	283.43	14.01
Duration of the mode t_e $[s]$	500	15000
DOD for Dimensioning [-]	0.90	0.90
Efficiency of LiIon Cells η_{LiIon} [-]	0.95	0.95
Required Battery Capacity per mode C_{mode} $[Wh]$	46.04	68.27
Total Required Battery Capacity $C_{\text{Batt,req}}$ $[Wh]$	**114.32**	

Table 4.3: Power consumption mode used as design case for the battery sizing.

Using these values a suitable battery cell and battery design configuration were conducted. Under consideration of these parameters the battery capacity C_{Batt} can be calcuated:

$$C_{\text{Batt}} = C_{\text{cell}} \cdot V_{\text{cell}} \cdot N \cdot M. \quad (4.2)$$

According to the ECSS reliability restrictions 1 battery string must be substracted for dimensionsing. Furthermore a 30% margin on the energy content was applied. This leads to a final battery configuration with a capacity of $C_{\text{Batt}} = 138{,}88\ Wh$ and a mass of $m_{\text{Batt}} = 1980\ g$. The final battery values are listed in Table A.1 [14].

4.5.4 EPS Power Control and Distribution

In order to ensure the full functionality of the EPS, the last main component to be selected is a suitable PCDU. As described in Figure 4.1, the PCDU forms the heart of the EPS and is an important interface to the OBC and COMM. Furthermore the PCDU shall be able to monitor and control the rover system if necessary through watchdogs, HPC (High Priority Commands) and direct connections to the OBC and COMM.
The PCDU has the challenging task not only to process the RTG as the main energy source, but also to process solar cells as secondary energy sources. Therefore, a PCDU was sought which has the required size, dimensions and range of functions. The research resulted in the Nova PCDU from Bradford DSI. In addition, margins were added to the PCDU to ensure feasibility[15].

4.6 Radiation

Compared to the radiation environment near Earth the radiation environment near Jupiter is multiple times stronger. It has the highest radiation levels of any planet in our solar systems [**Platzhalter**]. In order to survive these harsh environmental conditions, special emphasis must be placed on the radiation protection. In Figure B.2, the average trapped proton and electron fluxes on Europa's orbit around Jupiter are shown in comparison to the outer Van Allen radiation belt around Earth. However, in contrast to the Van Allen radiation belt, the duration within the radiation environment on Europa cannot be minimised and the rover has to be designed to withstand the entire mission duration of 30 days.

In oder to design and evaluate different radiation protection approaches, different calculations have to be performed. For this purpose the ESA SPace ENVironment Information System (SPENVIS) is used [**Platzhalter**]. All calculations and figures in Section 4.6 are performed with SPENVIS unless otherwise stated.

4.6.1 Radiation Protection

Various options are available to protect the rover against the radiation. A common approach is the use of aluminium or titanium as these materials can also act as structural elements. However, due to the mass constraints of 30 kg other materials or material compositions are taken in consideration which are more mass effective. In Table 4.4, an optimised shield structure is presented for different weight thresholds designed for the radiation environment around Jupiter.

The difference between an aluminium or titanium shielding and an optimised structure listed in Table 4.4 for the total ionizing dose (TID) is shown in Figure B.3.

Due to the mass savings of the optimised structure it will be used where the radiation protection of the aluminium structure is not sufficient. In order to reduce the mass further, a radiation vault is utilised that highly sensible components do not have to be shielded separately.

Table 4.4: Optimal shield structure for an Jupiter mission. [**Platzhalter**]

Areal Density / g/cm^2	0.5	1	2	3
Layer No. 1 / mm	Pb 0.415	Pb 0.829	W 0.984	Ta 1.563
Layer No. 2 / mm	Fe 0.033	Mg 0.158	Mg 0.540	Al 0.399
Layer No. 3 / mm	- -	- -	- -	Mg 0.150

4.6.2 Components

Every component on the rover has a different radiation tolerance and therefore have to be placed at different compartments within the rover. The radiation tolerances are listed in Table B.2. None sensitive components like the electric motors and harness are only shielded by an aluminium structure where components like the metal within the wire are resistant against the radiation. However, isolators around the cables have to be selected to be resistant in order to prevent short circuits. Highly sensitive components like cameras have an additional protective layer in order to reduce the TID to under 30 krad. Components which are within the rover like the on-board computer (OBC) are placed within the radiation vault which reduces the TID to under 20 krad. For this purpose the optimised shield structure with a weight target of 0.5 g/cm^2 is used. Detailed TIDs for all components are shown in Figure B.4.

4.6.3 Improvements

Even though the radiation protection is sufficient for the rover to survive at least the nominal mission of 30 days, further improvements can be performed in order to extend the secondary mission.

Local shielding can be applied on less resistant components in order to reduce the wall thickness of the whole radiation wall. If components with a radiation tolerance under 43.27 krad are individually shielded a mass saving of 736.2 g can be achieved. Additionally, water ice extracted from the surface of Europa can be used to improve the radiation protection. With a layer of one centimetre of water, the TID within the radiation vault can be reduced to 16.03 krad without the additional radiation protection beside the 4 mm of aluminium structure. The start mass of the rover can therefore be reduced by 897.2 g by removing the additional shielding.

Detailed calculations for local shielding and water improvements can be found in Appendix B.3 and may be analysed further in Phase B.

4.6.4 Conclusion

In order to protect the rover against the high radiation levels at the surface of Europa, the rover has different compartments. High sensible components are placed within a radiation vault which has a mass optimised structure. Components which has to be outside the radiation vault but are highly sensible are shielded individually. Low sensible Components are protected by the Aluminium structure. Figure 4.2 illustrates the different compartments within the rover and the accorded TIDs.
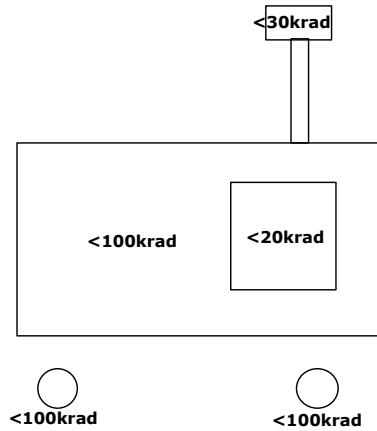
Figure 4.2: Overview of TIDs within different compartments within the rover.

4.7 Locomotion

The locomotion subsystem deals with the aspect of how the rover moves and the technical design, including the selection of components such as motors or gearboxes. Before the components can be determined, however, it is necessary to consider certain parameters and design drivers. These will be introduced in the following, and the decisions or estimations concerning the rover will be presented.

4.7.1 Design drivers for Rover Classification

The first consideration in designing a rover is the environmental and operational conditions expected for the mission operation. The ice moon can be assumed to have a solid surface; thus, a wheeled rover is chosen. Further design drivers that led to the locomotion mobility systems are based on a tradeoff presented a tradeoff in Figure D.7. However, the main design drivers are briefly summarised in Table 4.5.

Table 4.5: Design Drivers for the rover movement technique regarding the environmental conditions on Europa and operating conditions.

Wheeled System	4-Wheels
One of the most common types of platform	Compared to 2-wheels:
- high level of experience	- stability can be ensured → important for drilling
- high TRL	- MMP decreases
Compared to other systems:	Compared to 6-wheels:
- analysis quite straightforward	- less complex → simplification
- simplification → one of the most critical design drivers	- mass can be reduced
All-Wheel Drive	All-Wheel Actuation
- traction can be increased	- reduces the risk of slippage on ice
- increase of DP and the slope angle θ	

With the configured rover, the resulting wheel formula is 4 x 4 x 4. The normal force on Europa can be calculated to:

$$W = m_{\text{total}} \cdot g_{\text{Europa}} = 39.45\,\text{N}\,. \tag{4.3}$$

Since each wheel is individually driven and controllable, the parameters in the following are designed for one wheel; the normal force per wheel is correspondingly $W_{\text{wheel}} = 9.8625$ N

4.7.2 System Parameters

Regarding techniques of rover movement, it is crucial to consider the local conditions in which the rover will be operating. The surface of Europa can be assumed to be mainly covered by ice. However, since there are also geysers that transport water to the surface, surface areas may be covered by snow. Though Europa's surface temperature does not exceed 130 K, rather icy, hard-packed snow can be assumed. For this study, a conservative design of the rover is considered, whereby material parameters of snow in Sweden were selected, shown in Figure D.8. Furthermore, the parameters depend on the width and diameter of the wheels of the rover. Therefore, several sizes dependent on the respective weight were selected and a limit per wheel was set to 200 g, illustrated in Figure D.9.
This constraint results in 6 configurations considered for the Rover system design, listed in Table 4.6.

Table 4.6: Configurations for Rover Classification respective to the wheel width bw, wheel diameter d_w and weight per wheel m_w

Configuration	bw /m	Diameter d_w /m	Weight m_w /kg
1	0.05	0.1	0.127
2	0.06	0.1	0.153
3	0.07	0.1	0.178
4	0.05	0.125	0.154
5	0.05	0.125	0.185
6	0.05	0.15	0.185

Mean Maximum Pressure
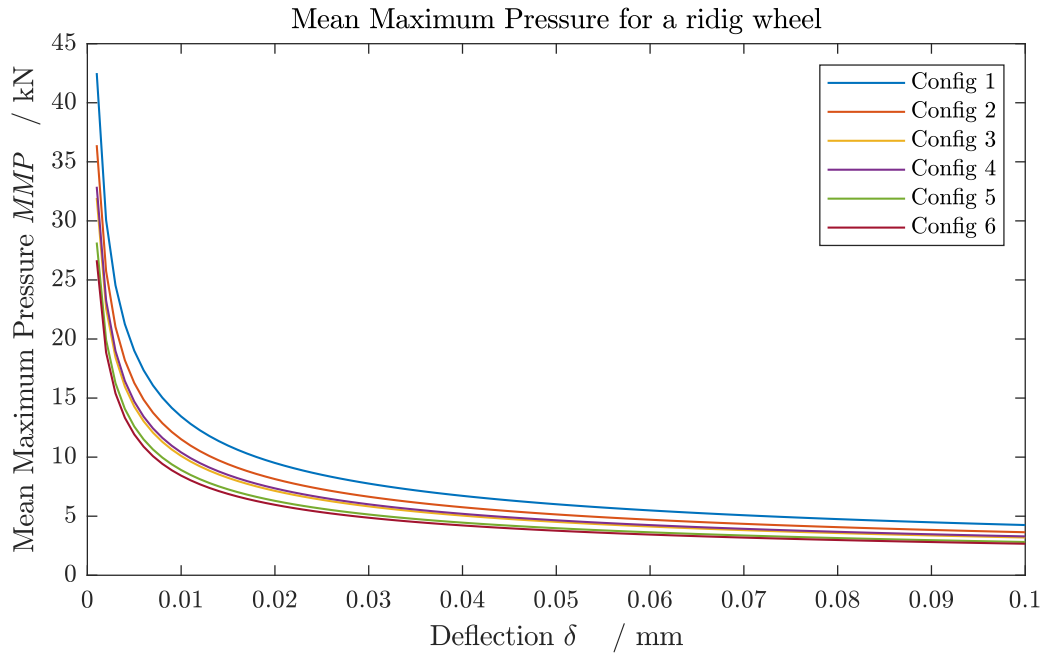
Figure 4.3

Drawbar Pull

Steering

Hardware Selection

4.7.3 Deployment mechanism

4.8 Control and Autonomy

Sinkage vs Slope Angle Gradeability

Figure 4.4

DrawbarPull vs Slope Angle Gradeability
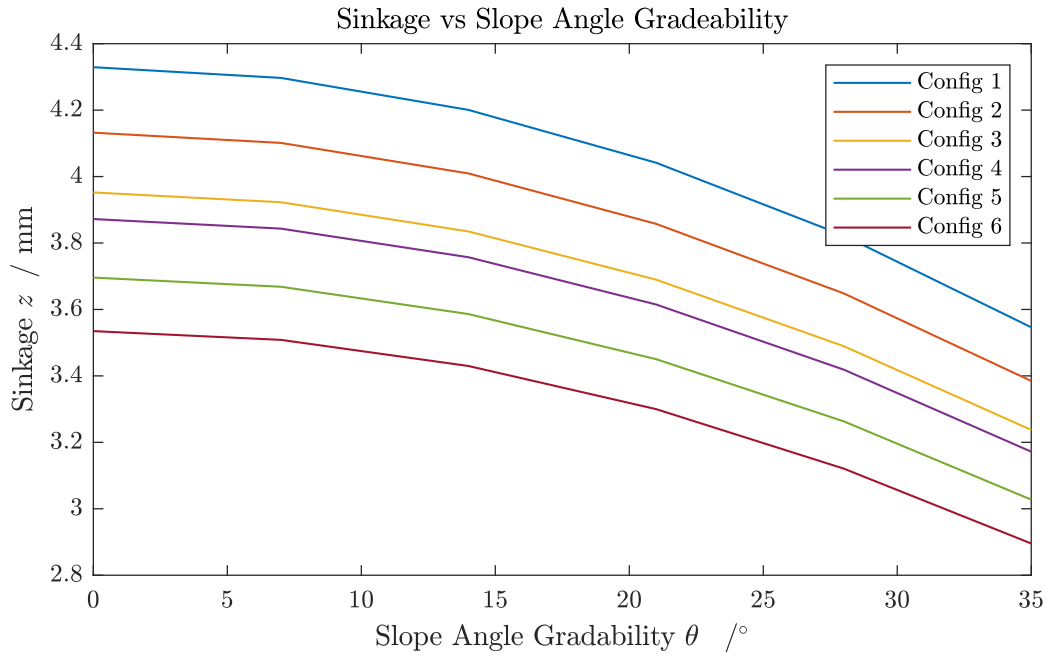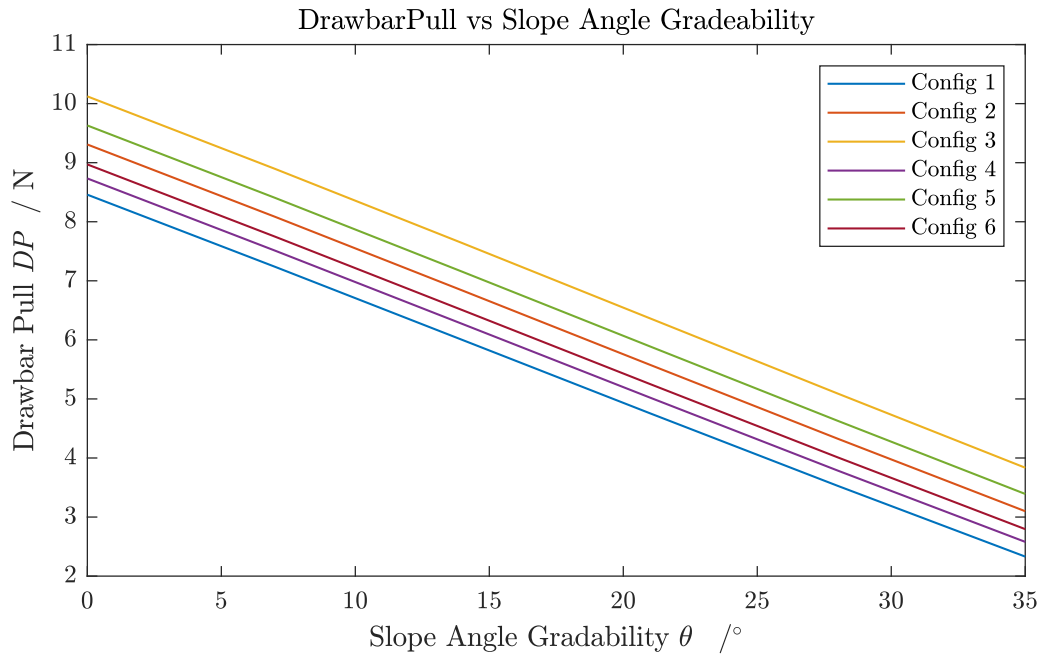
Figure 4.5

4.9 Thermal Control System

The main object of the Thermal Control System (TSC) is to keep the eletric components within their temperature limits, listed in Table E.8. As a result of Europas low ground temperature, a small solar constant and the thin atmosphere the heat loss of the rover has to be minimised. This shall be reached by a smart heat distribution as well as by an adequate insulation and surface finishing.

4.9.1 Concepts

The main heat source of the rover is the waste heat of the RTG (see Section 4.5), which will be lead by thermal straps to the thermal critical components. The first attempt to use straps made out of copper was rejected du to the high resulting mass. Therefore, carbon-based straps $LyNX^{®}$ with a high thermal conductivity to density ratio will be used, [16]. However, the thermal conductivity is highly depend on the materials temperature, see Figure 4.6. The curve was aproximated by an qubic interpolation, autoref appendix. To consider heat loss as a result of surface contact and radiation, the thermal conductivity was reduced about 20%.
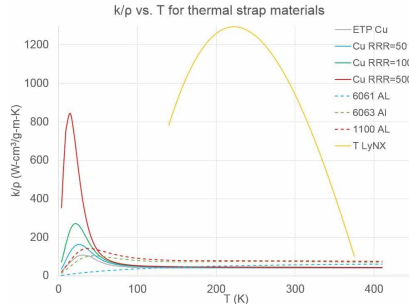
(a) Temperature dependent thermal conductivity/density of $LyNX^{®}$ (yellow curve), copper, and aluminum, [16].
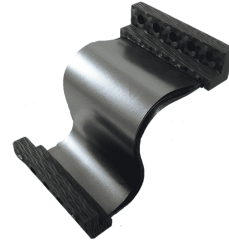
(b) Example of a thermal strap, [16].

Figure 4.6: Carbon-based thermal strap $LyNX^{®}$.

The camera, exposed on a mast, will be heated by a seperate, light weight Radioisotope Heater Unit (RHU), which has been used during several NASA missions, [17]. For the insulation, the material *aerogel* will be applied, which has a very low heat conductivity ($0.016 - 0.03\frac{W}{mK}$) as well as a low density ($5 - 200\frac{kg}{m^3}$) and has also been used in space applications [18].

A surface finishing with an low emisivity is necessary. For the most componets, a cost-efficient surface polishing is applicable. The camera will get a special white paint with a high absorptivity to gather the sun light.

But there is also a risk of overheating, because of the lack of heat convection. This circumstance concern the engines and also the camera. To get rid of the extensive heat and to prevent the damage of the components special bi-metallic heat switches will be placed (see Figure 4.7). These switches change their heat conductivity beyond a certain temperatur due to the expansion of the disk (see Figure 4.8). It was assumed, that the toggle temperatur can be adapted by increasing the disk height. The influence of the changed disk stiffens on the contact pressure and the heat conductivity was neglected for this study. The measured heat conductivity characterisitc was divided in three linear sections (Figure 4.8b), to enable a simple modelling in the upcoming thermal calculation.

16

(a) Closed switch, high heat conduction.

(b) Open switch, reduced heat conduction.
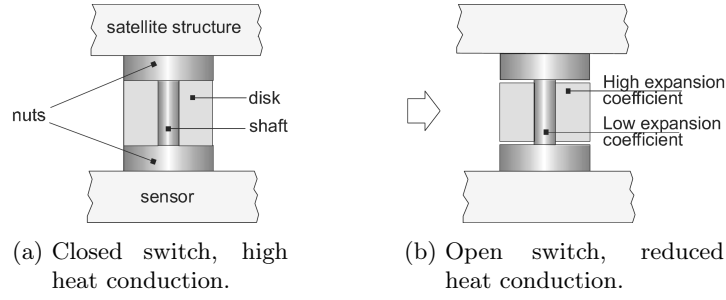
Figure 4.7: Bi-metallic heat switch, [19].

(a) Comparison between data and theory (experimental results), [19]

(b) Linearised characteristic of bi-metallic heat switch.
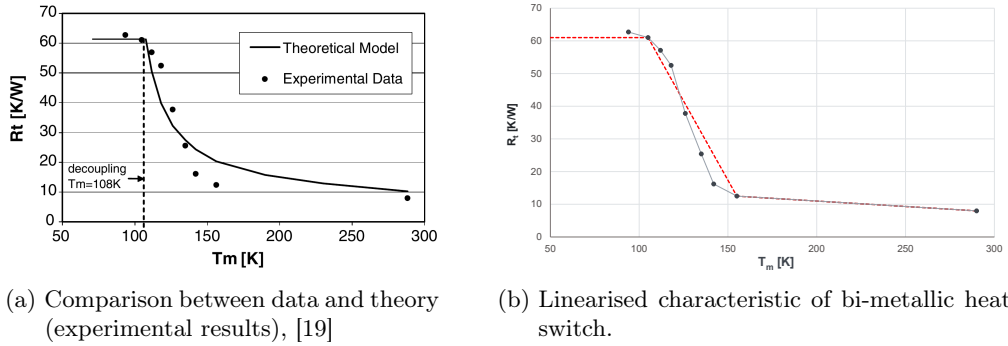
Figure 4.8: Change of the heat switch conductivity R_t over the mean temperature T_M.

4.9.2   Thermal Network

A thermal analysis was performed in order to get

- the dimension of the isnulation and heat straps,

- the necessary amount of RHUs and heat switches,

- the required surface finishing and

- the suitable choice of material.

For that, a thermal network with ten nodes was derived from the rover, shown in Figure 4.9. At the intersection of the steering and drive engien, two additional nodes were defined to calculate the heat flow.
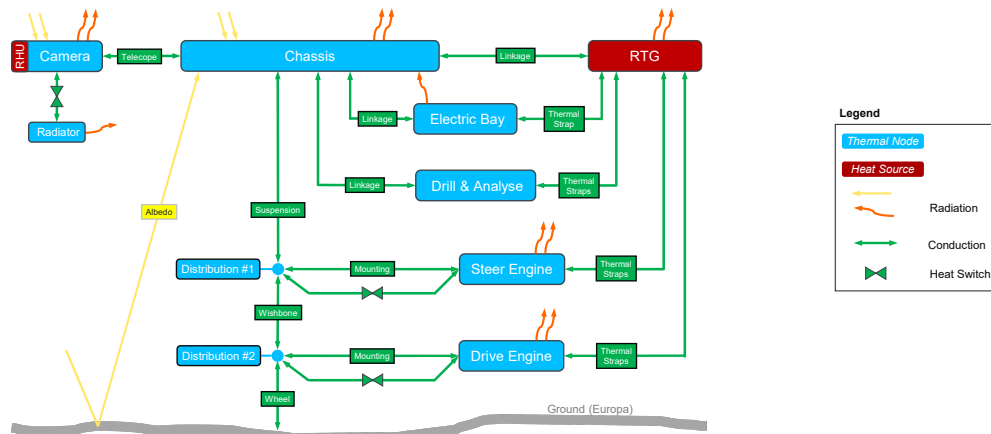
Figure 4.9: Thermal network of the rover.

On the basis of the thermal network, the heat energy equlibrium for each node was defined (see Subsection E.1). The calculation were considered as a quasi-static analysis, were the component temperatures stay constant, $\frac{\mathrm{d}T}{\mathrm{d}t} = 0$. Due to the early state of the rover, simplifications and asumptions for the analysis were made.

- The convection was neglected due to the thin atmosphere.

- The whole electrical power of the components will be dissipated into heat.

- A variation of $\pm 20\%$ for the emisivity and absorpsivity values was considered, if applicable (seet Table E.9).

- The heat as a result of retardation radiation inside the shielding was neglected.

- No dicrete nodes for the radar, hazcams and deployment engines were considered. Their heat will be lead into the chassis.

- The thermal resistance between two surfaces and ther radiation of the thermal strap was neglected. To compensate this assumption, the heat conductivity was reduced about 20%.

4.9.3 Analysis

The thermal analysis was perfomred as a Excel calculation, which can be found in the corresponding folder of Team 3. The calculation sheet offers the possibility to adapt and customise input values and dimension.

4.9.4 Results

The results of the temperatures for each node for the hot and cold cases are listed in Table 4.7. The temperature margins for uncertainties, acceptance tests and qulification tests were considered with $5K$ each, $\pm 15K$ in total. The corresponding temperatures are listed in autoreftab:. All temperature lay betwenn their limits without using a heater. Nevertheless, heaters were considered for the power calculation, see Section 4.5.

Table 4.7: Temperature results in K of thermal analysis, including a margin of $\pm 15K$.

Components	Load Case				
	Hot case			Cold case	
	$0K$	$+15K$		$0K$	$-15K$
RTG	380	395		350	335
Electric Bay	310	325		261	246
Drill & Analyser					
Camera					
Steering Engine					
Drive Engine					

In a furher step, a more detailed analysis should to be carried out with the Finite-Element-Method to identify the correct heat and temperature distribution. The FE results could be used to verify and adjust the analytical analysis to get a helpful tool for fast thermal calculation to evaluate different materials or desings in the further development phases. A transient analysis could also help to optimise the insulation design. The current thermal configuration for the engine is defined for a continuous operation

Chapter 5

Outlook

Bibliography

[1]   Jet Propusion Laboratory. *Galileo Mission to Jupiter*. [online] \url{https://www.jpl.nasa.gov/missions/galileo}.

[2]   NASA Science. *Europa Ocean Moon*. [online] \url{https://solarsystem.nasa.gov/moons/jupiter-moons/europa/in-depth/}.

[3]   Institut für Planetenforschung, DLR. *Die Mission JUICE zum Jupitersystem*. [online] \url{https://www.dlr.de/pf/desktopdefault.aspx/tabid-10617/18438_read-43016/}.

[4]   NASA. *Europa Lander*. [online] \url{https://europa.nasa.gov/}.

[5]   NASA / JPL. *Europa*. [online] \url{https://www.jpl.nasa.gov/missions/europa-lander}.

[6]   Fraunhofer Institute for Solar Energy Systems ISE. *RadHard Project Website*. 2021. [online] \url{https://radhard.org/}.

[7]   R. Abelson et al. *Enabling Exploration with Small Radioisotope Power Systems*. Ed. by NASA JPL. 2004.

[8]   S. Magdum. *Model Based Development of The Enhanced Multi-Mission Radioisotope Thermoelectric Generator and Effect of Thermoelectric Element Length on eMMRTG*. Ed. by Western Michigan University. 2019. [online] \url{http://homepages.wmich.edu/~leehs/ME539/Final%20Presentation%20on%20eMMRTG.pdf}.

[9]   Holgate, T. C.; Bennett, R.; Hammel, T.; Caillat, T.; Keyser, S., and Sievers, B. "Increasing the Efficiency of the Multi-mission Radioisotope Thermoelectric Generator". In: *Journal of Electronic Materials* 44.6 (2015), pp. 1814–1821. ISSN: 0361-5235. DOI: \url{10.1007/s11664-014-3564-9}.

[10] JPL NASA. *Enhanced Multi-Mission Radioisotope Thermoelectric Generator (eMMRTG) Concept*. Ed. by NASA JPL. 2014. [online] \url{https://rps.nasa.gov/resources/56/enhanced-multi-mission-radioisotope-thermoelectric-generator-emmrtg-concept/}.

[11] Lakdawalla, E. *The Design and Engineering of Curiosity*. Cham: Springer International Publishing, 2018. ISBN: 978-3-319-68144-3. DOI: \url{10.1007/978-3-319-68146-7}.

[12] S. Fasoulas et al. *Lecture Series: Energy Systems for Space Application SS 2020*. 2020.

[13] S. Klinkner; P. Winterhalder, and M.Nitz et al. *Lecture Series - Rover System Technology SS2021*. 2021.

[14] SAFT Batteries. *Datasheet - SAFT MP 176065 xlr*. 2018. [online] \url{https://www.saftbatteries.com/products-solutions/products/mp-small-vl}.

[15] Bradford Space. *Datasheet - Nova PCDU*. Ed. by BRADFORD ENGINEERING BV. 2019. [online] \url{https://satsearch.co/products/bradford-nova-pcdu}.

[16] Thermal Space and Thermal Straps. *Graphene Thermal LyNX® Technology*. [online] \url{https://thermal-space.com/thermal-lynx/}.

[17] NASA. *Light-Weight Radioisotope Heater Unit*. [online] \url{https://rps.nasa.gov/power-and-thermal-systems/thermal-systems/light-weight-radioisotope-heater-unit/}.

[18] NASA / JPL. *Aerogel*. [online] \url{https://solarsystem.nasa.gov/stardust/aerogel_factsheet.pdf}.

[19]   Milanze, F. H. and Mantelli, M. B. "Theoretical and experimental studies of a bi-metallic heat switch for space applications ". In: *International Journal of Heat and Mass Transfer* 46.24 (2003), pp. 4573–4586. ISSN: 0017-9310. DOI: `https://doi.org/10.1016/S0017-9310(03)00294-1`.

Appendix

A   Electrical Power System

SAFT 176065 xlr [14]	
Configuration:	
Battery Configuration	$4s3p$
Cells in Sereis s N [-]	4
Cells in Parallel p M [-]	3
Cell Parameters:	
Typical Cell Capacity $[Ah]$	6.8
Nominal Cell Voltage $[V]$	3.65
Nominal Cell Capacity $[Wh]$	24.8
Typical Cell Mass $[kg]$	0.15
Energy Density $[Wh/kg]$	165.33
Actual Battery Configuration Parameters:	
Battery Voltage V_{Batt} [V]	14.6
Battery Nominal Capacity E_{Batt} $[Wh]$	297.6
Battery Mass $[kg]$	1.8
Battery Mass m_{Batt} (incl. 10% Margin) $[kg]$	**1.98**
Configuration according to ECSS reliability restrictions and margins included:	
Battery Configuration	$4s2p$
Cells in Sereis s N [-]	4
Cells in Parallel p M [-]	2
Battery Voltage V_{Batt} $[V]$	14.6
Battery Nominal Capacity E_{Batt} $[Wh]$	198.4
30% Margin on Energy Content	0.3
Battery Nominal Capacity E_{Batt} incl. Margin $[Wh]$	**138.88**
Useable Energy Density $[Wh/kg]$	70.14

Table A.1: INSPIRE battery parameters.

B   Radiation

In this chapter, detailed calculations are performed on which Section 4.6 is based on. All calculations and figures in Section B are performed with SPENVIS unless otherwise stated. In order to simulate the radiation on Europa an orbit around Jupiter is simulated with the orbit parameters of Europa with a total mission duration of 30 days. The chosen parameters were an perijove altitude of 664,862 km, an apojove altitude of 676,938 km, and an inclination of 0.47°.

Subsystem	Unit	Amount [-]	Maturity Level Margin [%]	Power demand per Unit			EDL			Deployment Mode			Idle/ Perception			Safe/ Hibernation			Communication			Charging (RTG)			Locomotion			Payload: Observation			Payload: Ice Core Mode		
				Standby (SB)	ON Nominal (ON)	ON Max (MAX)	Status	Duty Cycle	Power [W]	Status	Duty Cycle	Power [W]	Status	Duty Cycle	Power [W]	Status	Duty Cycle	Power [W]	Status	Duty Cycle	Power [W]	Status	Duty Cycle	Power [W]	Status	Duty Cycle	Power [W]	Status	Duty Cycle	Power [W]	Status	Duty Cycle	Power [W]
Payload																																	
	Ice Core Drill	1	20,00%		1	15	OFF			OFF		0	OFF		0	OFF		0	OFF		0	OFF		0	OFF		0	OFF		0	MAX	50%	0,6
	APXS Analyser	1	5,00%	0	0,15	1,5	OFF			OFF		0	OFF		0	OFF		0	OFF		0	OFF		0	OFF		0	OFF		0	MAX	50%	0,7875
	Stereo Vision Camera	2	5,00%	0	2	4	OFF			ON	100%	4,2	ON	25%	1,05	OFF		0	OFF		0	OFF		0	ON	100%	4,2	ON	100%	4,2	OFF		0
	Hazcams	4	5,00%	0	2	4	OFF			ON	100%	8,4	ON	25%	2,1	OFF		0	OFF		0	OFF		0	ON	100%	8,4	OFF		0	OFF		0
	Ground RADAR	1	10,00%	0	0,3	3	OFF			OFF		0	OFF		0	OFF		0	OFF		0	OFF		0	OFF		0	MAX	25%	0,825	OFF		0
	LED Lampe	8										0			0			0			0			0			0			0			0
Command & Data Handling												0			0			0			0			0			0			0			0
	Processor	1	5,00%	1	8	10	OFF			ON	100%	8,4	MAX	90%	9,45	OFF	0%	0	ON	100%	8,4	ON	5%	0,42	ON	100%	8,4	ON	100%	8,4	ON	100%	8,4
												0			0			0			0			0			0			0			0
												0			0			0			0			0			0			0			0
Thermal Control System												0			0			0			0			0			0			0			0
	Heaters	2	5,00%	0	1	2	ON	100%	2,1	ON	100%	2,1	ON	100%	2,1	ON	100%	2,1	ON	100%	2,1	ON	85%	1,785	ON	100%	2,1	ON	100%	2,1	ON	100%	2,1
												0			0			0			0			0			0			0			0
Electric Power Supply									0			0			0			0			0			0			0			0			0
	PCDU	1	10,00%	0,6	1	1	SB	100%	0,66	SB	100%	0,66	ON	100%	1,1	SB	100%	0,66	ON	100%	1,1	SB	100%	0,66	ON	100%	1,1	ON	100%	1,1	ON	100%	1,1
												0			0			0			0			0			0			0			0
												0			0			0			0			0			0			0			0
Communication												0			0			0			0			0			0			0			0
	Transmitter	1	10,00%	0,6	10	15	OFF			OFF		0	OFF		0	OFF		0	MAX	100%	16,5	OFF		0	OFF		0	OFF		0	OFF		0
	Receiver	1	10,00%	0,35	1	2	OFF			ON	100%	1,1	ON	100%	1,1	ON	100%	1,1	MAX	100%	2,2	SB	100%	0,385	ON	100%	1,1	ON	100%	1,1	ON	100%	1,1
Locomotion												0			0			0			0			0			0			0			0
	Motor (wheels)	4	5,00%	0	30	45	OFF			OFF		0	OFF		0	OFF		0	OFF		0	OFF		0	MAX	100%	126	OFF		0	OFF		0
	Motor (steering)	4	5,00%	0	15	15	OFF			OFF		0	OFF		0	OFF		0	OFF		0	OFF		0	MAX	10%	6,3	OFF		0	OFF		0
	IMU	10	5,00%									0			0			0			0			0			0			0			0
												0			0			0			0			0			0			0			0
Chassi & Structure												0			0			0			0			0			0			0			0
	Rover Boogie Depolyment											0			0			0			0			0			0			0			0
	Drill Mechanism											0			0			0			0			0			0			0			0
												0			0			0			0			0			0			0			0

S/C Net Power Demand [W]	Margin [%]			2,76		24,86		16,90		3,86		30,30		3,25	157,60	17,73	14,09
Power Distribution loss	2,00%			0,06		0,50		0,34		0,08		0,61		0,07	3,15	0,35	0,28
Load Discharge (PCDU)	7,00%			0,19		1,74		1,18		0,27		2,12		0,23	11,03	1,24	0,99
PCDU Margin (Conversion etc.)	5,00%			0,14		1,24		0,85		0,19		1,52					
Harness losses	3,50%			0,10		0,87		0,59		0,14		1,06		0,11	5,52	0,62	0,49
Additional losses ...	5,00%			0,14		1,24		0,85		0,19		1,52		0,16	7,88	0,89	0,70
S/C Brutto Power Demand [W]				3,38		30,45		20,70		4,73		37,12		3,82	185,18	20,83	16,55
System Margin	20,00%			0,68		6,09		4,14		0,95		7,42		0,76	37,04	4,17	3,31
Required power from Battery (20% System Margin) [W]				4,06		36,54		24,84		5,67		44,54		4,58	222,22	24,99	19,86
Total Rover Power Demand excluding battery charge (Battery Charge loss 5% + LiIon Efficiency 5%) [W]	10,00%			4,46		40,20		27,33		6,24		49,00		5,04	244,44	27,49	21,85
Incoming Power RTG				12,08		12,08		12,08		12,08		12,08		12,08	12,08	12,08	12,08
Total Rover Power Demand including battery charge [W]				-7,62		28,12		15,25		-5,84		36,92		-7,04	232,36	15,41	9,77

Figure A.1: POWER BUDGET DUMMY!

B.1 Jupiters Radiation Environment

In order to compare the radiation environment around Jupiter and the radiation environment around Earth the following trapped radiation models were used: for Jupiter the D&G83+Salammbo proton model and D&G83+GIRE+SalammboE electron model was used; for Earth the AP-8 proton model and the AE-8 electron model was used.

(a) Average spectra of trapped electrons around Earth

(b) Average spectra of trapped protons around Earth

(c) Average spectra of trapped electrons around Jupiter

(d) Average spectra of trapped protons around Jupiter

Figure B.2: Average trapped proton and electron fluxes on an orbit around earth at 25,000 km, through the outer Van Allen radiation belt, and on Europa's orbit around Jupiter.

B.2 Radiation Exposures

In order to simulate the TID for different radiation protections the Geant4 tool Multi-Layered Shielding Simulation (MULASSIS) is used. As target material silicon is selected with a thickness of 1 μm. As shape a planar slap is selected because of the ice ground on one side of the rover.

(a) TID for Electrons as Source Particles   (b) TID for Protons as Source Particles
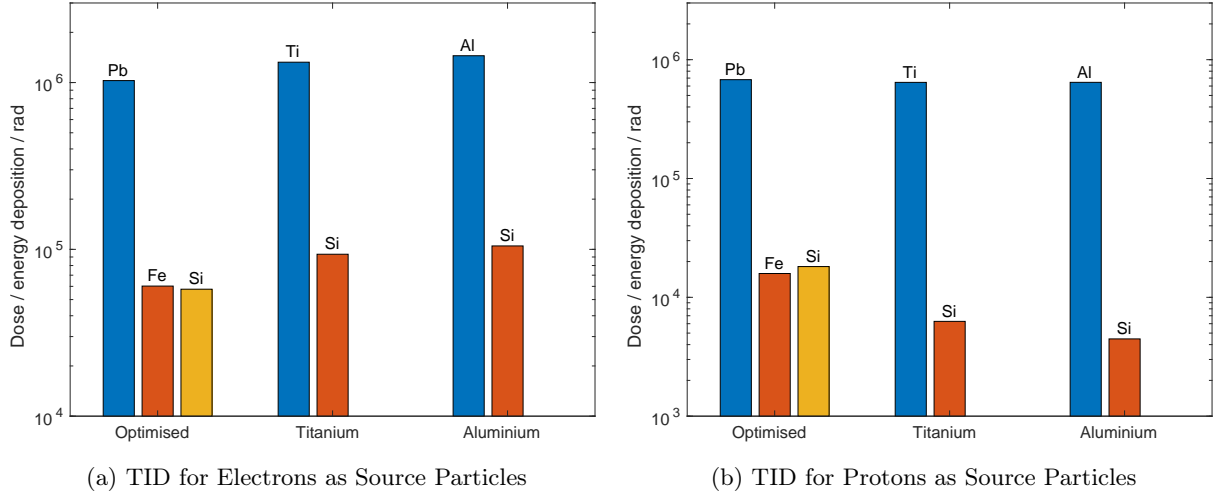
Figure B.3: TID of aluminium, titanium, and the optimised radiation structure shown in Table 4.4 with a weight target of all three structures of 0.5 g/cm^2 over 30 days of exposure on Europa.

Table B.2: Used components and the respective radiation tolerance and location

Components	Rated TID	Exposed TID	Location
Electric Motors	-	< 205 krad	locomotion housing
Harness	-	< 98 krad	chassis
Stereo Vision Cams	40	< 31 krad	camera housing
OBC	1000	< 17 krad	E-Bay
PCDU	20	< 17 krad	E-Bay

(a) TID for Electrons as Source Particles

(b) TID for Proton as Source Particles
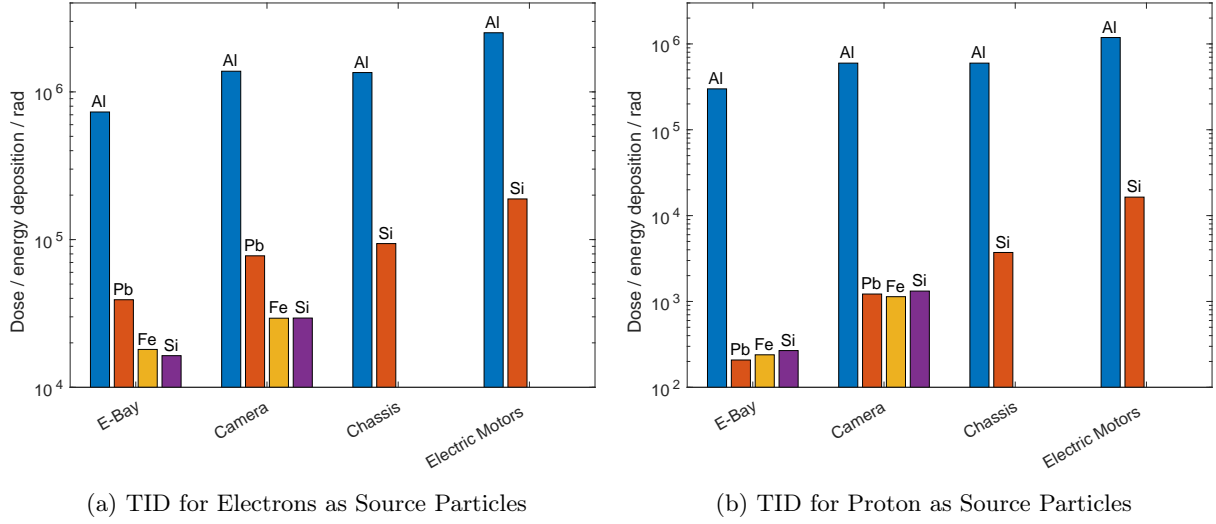
Figure B.4: TID for different compartments as seen in Figure 4.2. The E-Bay is shielded by 4 mm aluminium, 0.415 mm lead, and 0.033 mm iron; the camera compartment by 2 mm aluminium, 0.415 mm lead, and 0.033 mm iron; the chassis by 2 mm aluminium; the electric motors by 1 mm aluminium.

B.3 Improvements

All simulations of the improvements introduced in Subsection 4.6.3 are performed in the same way as in Subsection B.2.

In Figure B.5, the TID over 30 days within the E-Bay is shown. If all components with an radiation resistance under 43.27 krad are shielded individually, the additional shielding structure around the E-Bay can be removed and the aluminium structure would be sufficient.
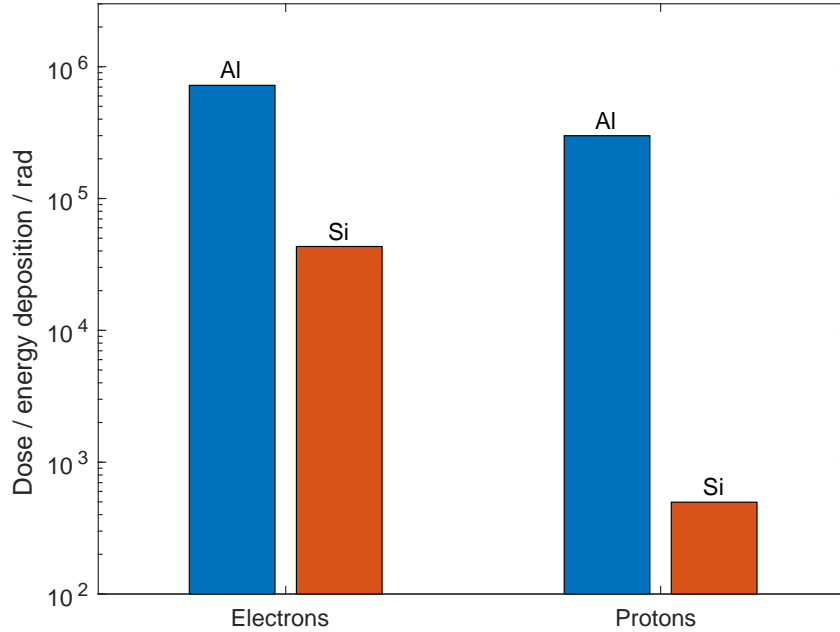
Figure B.5: TID with 4 mm Al shielding over a mission duration of 30 days

The resulting mass savings can be calculated with Equation 5.1 with m^* as the specific weight of the radiation protection and N as the amount of components within the E-Bay with a radiation

resistance under 43.27 krad as of Table B.2.

$$\Delta m = SA_{\text{E-Bay}} \cdot m^*_{\text{Shielding}} - \sum_{n=0}^{N} SA_{\text{Component, n}} \cdot m^*_{\text{Shielding}} \tag{5.1}$$

With inserted values this results in a mass saving of $\Delta m = 736.2$ g.
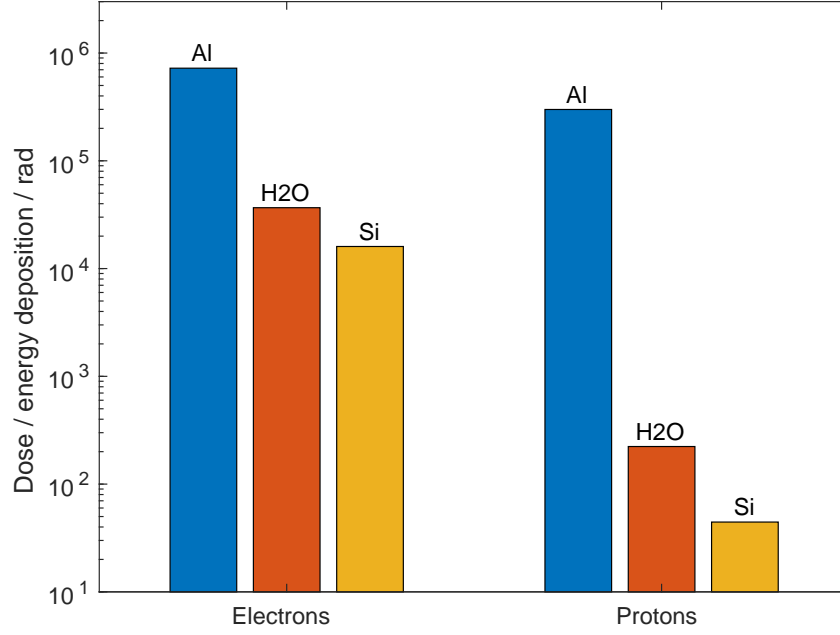
Figure B.6: TID with 4 mm Al shielding and 1 cm of Water over a mission duration of 30 days

Parameter	Var	Vlaue	Unit	source
Rover Antenna Gain	{G}_{r}		[dB]	
Rover Output Power	{P}_{r}		[W]	
Rover Line Loss			[dB]	
R2L polarization loss			[dB]	
Path loss			[dB]	
Atmospheric loss			[dB]	
Lander Antenna Gain	{G}_{L}		[dB]	
Lander Pointing Loss			[dB]	
Lander Line Loss			[dB]	
eff. noise temperature			[K]	
data rate			[kbps]	
FEC coding			[-]	
technical degradation			[dB]	
implementation loss			[dB]	

C Communications

C.1 Link Budget

Link budget considerations have been performed under the conservative assumptions listed in table

$$\frac{E_b}{N_0} = G_t + P_t + G_r + k_{boltzmann} + L_{line} + L_{atmosph.} + L_{polarisation} + L_{pointing} \qquad (5.2)$$

D Locomotion

D.1 Locomotion Design Drivers

criteria	mass	low complexity	TRL	energy efficiency	traction	sum	weighting factor [%]
mass		+	+	0	0	2	28.6%
low complexity	-		+	-	-	1	14.3%
TRL	0	-		+	-	1	14.3%
energy efficiency	0	+	-		0	1	14.3%
traction	0	+	+	0		2	28.6%
Total number of "+"						7	
weighting of one "+" [%]							14.3%

| | | | locomotion systems | | | | | | |
criteria	weighting factor	4 wheels		6 wheels		tracks		legs	
mass	28.6%	2.00	0.57	1.00	0.29	0.00	0.00	1.00	0.29
low complexity	14.3%	2.00	0.29	1.00	0.14	1.00	0.14	0.00	0.00
TRL	14.3%	2.00	0.29	2.00	0.29	1.00	0.14	0.00	0.00
energy efficiency	14.3%	2.00	0.29	2.00	0.29	1.00	0.14	1.00	0.14
traction	28.6%	1.00	0.29	1.00	0.29	2.00	0.57	1.00	0.29
max. percentage	100.0%	9.00	1.71	7.00	1.29	5.00	1.00	3.00	0.71
sum	max. 2,00	1.71		1.29		1.00		0.71	
rank		1		2		3		4	

Legende	
Pkt.	%
2	>80
1	>40
0	<40

Figure D.7: Trade-off of the locomotion movement system. The criteria with the respective weighting factors are shown on the left. On the right side are the respective systems.

Terrain	Moisture Content (%)	n	k_c lb/in.$^{n+1}$	k_c kN/m^{n+1}	k_ϕ lb/in.$^{n+2}$	k_ϕ kN/m^{n+2}	c lb/in.^{2}	c kPa	ϕ deg
Dry sand (Land Locomotion Lab., LLL)	0	1.1	0.1	0.99	3.9	1528.43	0.15	1.04	28°
Sandy loam (LLL)	15	0.7	2.3	5.27	16.8	1515.04	0.25	1.72	29°
	22	0.2	7	2.56	3	43.12	0.2	1.38	38°
Sandy loam Michigan (Strong, Buchele)	11	0.9	11	52.53	6	1127.97	0.7	4.83	20°
	23	0.4	15	11.42	27	808.96	1.4	9.65	35°
Sandy loam (Hanamoto)	26	0.3	5.3	2.79	6.8	141.11	2.0	13.79	22°
	32	0.5	0.7	0.77	1.2	51.91	0.75	5.17	11°
Clayey soil (Thailand)	38	0.5	12	13.19	16	692.15	0.6	4.14	13°
	55	0.7	7	16.03	14	1262.53	0.3	2.07	10°
Heavy clay (Waterways Experiment Stn., WES)	25	0.13	45	12.70	140	1555.95	10	68.95	34°
	40	0.11	7	1.84	10	103.27	3	20.69	6°
Lean clay (WES)	22	0.2	45	16.43	120	1724.69	10	68.95	20°
	32	0.15	5	1.52	10	119.61	2	13.79	11°
LETE sand (Wong)		0.79	32	102	42.2	5301	0.19	1.3	31.1°
Upland sandy loam (Wong)	51	1.10	7.5	74.6	5.3	2080	0.48	3.3	33.7°
Rubicon sandy loam (Wong)	43	0.66	3.5	6.9	9.7	752	0.54	3.7	29.8°
North Gower clayey loam (Wong)	46	0.73	16.3	41.6	24.5	2471	0.88	6.1	26.6°
Grenville loam (Wong)	24	1.01	0.008	0.06	20.9	5880	0.45	3.1	29.8°
Snow (U.S.)		1.6	0.07	4.37	0.08	196.72	0.15	1.03	19.7°
(Harrison)		1.6	0.04	2.49	0.10	245.90	0.09	0.62	23.2°
Snow (Sweden)		1.44	0.3	10.55	0.05	66.08	0.87	6	20.7°

Figure D.8: Soil Parameters

D.2 Formulas for Locomotion Parameters

Wheel Width [m]	Wheel Diameter [m]	Weight per Wheel [g]
0.0500	0.1000	127
0.0600	0.1000	153
0.0700	0.1000	178
0.0800	0.1000	204
0.0900	0.1000	229
0.1000	0.1000	265
0.1500	0.1000	396
0.2000	0.1000	527
0.2500	0.1000	658
0.3000	0.1000	790
0.0500	0.1250	154
0.0600	0.1250	185
0.0700	0.1250	217
0.0800	0.1250	247
0.0900	0.1250	278
0.1000	0.1250	309
0.0500	0.1500	185
0.0600	0.1500	221
0.0700	0.1500	258
0.0800	0.1500	294
0.0900	0.1500	331
0.1000	0.1500	367
0.1500	0.1500	570
0.2000	0.1500	760
0.2500	0.1500	949
0.3000	0.1500	1138
0.0500	0.2000	236
0.0600	0.2000	284
0.0700	0.2000	332
0.0800	0.2000	379
0.0900	0.2000	427
0.1000	0.2000	487
0.1500	0.2000	730
0.2000	0.2000	973
0.2500	0.2000	1215
0.3000	0.2000	1458

Figure D.9: Various wheel dimensions respective to the weight. Rows highlighted in red are not considered further for system design due to the limit of 200 g weight per wheel.

E Thermal Controls System

E.1 Heat energy eqilibrium

The follwing equiations describe each node of the thermal network. The input values were tanken from EPS, Subsection E.2, Subsection E.3, Subsection E.4 respectively.

RTG:

$$0 = \dot{Q}_{RTG} + CON_1 \cdot (T_{Bay} - T_{RTG}) + CON_2 \cdot (T_{Chassis} - T_{RTG}) +$$

$$+ CON_5 \cdot (T_{Drill} - T_{RTG}) - \epsilon_{RTG} \cdot \sigma_b \cdot S_{RTG} \cdot T_{RTG}^4 \tag{5.3}$$

Electric Bay:

$$0 = \dot{Q}_{Bay} + CON_1 \cdot (T_{RTG} - T_{Bay}) + CON_3 \cdot (T_{Chas} - T_{Bay}) - \epsilon_{Bay} \cdot \sigma_b \cdot S_{Bay} \cdot T_{Bay}^4 \tag{5.4}$$

with:

$$\dot{Q}_{B,intern} = \dot{Q}_{C\&DH} + \dot{Q}_{Tranceiver} + \dot{Q}_{Receiver} + \dot{Q}_{PCDU} \tag{5.5}$$

Drill & Analyser:

$$0 = \dot{Q}_{Drill} + CON_4 \cdot (T_{Chas} - T_{Drill}) + CON_5 \cdot (T_{RTG} - T_{Drill}) \tag{5.6}$$

Camera:

$$0 = \dot{Q}_{Cam} + \dot{Q}_{RHU} + CON_6 \cdot (T_{Chas} - T_{Cam}) +$$

$$+ (CON_{14} + n_{S1} \cdot CON_{S1}) \cdot (T_{Rad} - T_{Cam}) - \epsilon_{Cam} \cdot \sigma_b \cdot S_{Cam} \cdot T_{Cam}^4 \tag{5.7}$$

Radiator:

$$(CON_{14} + n_{S1} \cdot CON_{S1}) \cdot (T_{Cam} - T_{Rad}) - \epsilon_{Rad} \cdot \sigma_b \cdot S_{Rad} \cdot T_{Rad}^4 = 0 \tag{5.8}$$

Chassis:

$$0 = \dot{Q}_{Radar} + \dot{Q}_{Hazcam} + CON_2 \cdot (T_{RTG} - T_{Chas}) + CON_3 \cdot (T_{Bay} - T_{Chas}) +$$

$$+ CON_4 \cdot (T_{Drill} - T_{Chas}) + CON_6 \cdot (T_{Cam} - T_{Chas}) + CON_7 \cdot (T_{Node_1} - T_{Chas}) +$$

$$+ \alpha_{Chas} \cdot [q_{Sun} \cdot (1 + \rho_E) \cdot (S_{Chas1} \cdot \varphi_1 + S_{Chas2} \cdot \varphi_2) + \epsilon_E \cdot \sigma_b \cdot S_{Chas3} \cdot T_{Surface}^4] - \tag{5.9}$$

$$- \epsilon_{Chas} \cdot \sigma_b \cdot S_{Chas} \cdot T_{Chas}^4$$

Steer Engine:

$$0 = 4 \cdot [\dot{Q}_{E,S} + (CON_8 + n_{S2} \cdot CON_{S2}) \cdot (T_{Node1} - T_{E,S}) +$$

$$+ CON_9 \cdot (T_{RTG} - T_{E,S}) - \epsilon_{E,S} \cdot \sigma_b \cdot S_{E,S} \cdot T_{E,S}^4] \tag{5.10}$$

Distribution Node 1:

$$0 = 4 \cdot [CON_7 \cdot (T_{Chas} - T_{Node_1}) + CON_8 \cdot (T_{E,S} - T_{Node_1}) +$$

$$+ CON_10 \cdot (T_{Node_2} - T_{Node_1})] \tag{5.11}$$
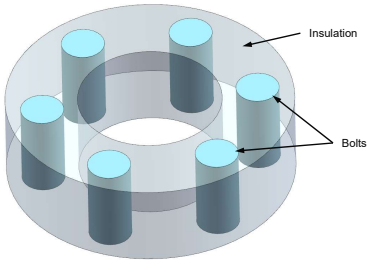
Drive Engine:

$$0 = 4 \cdot [\dot{Q}_{E,D} + (CON_{11} + n_{S3} \cdot CON_{S3}) \cdot (T_{Node_2} - T_{E,D}) +$$

$$+ CON_{12} \cdot (T_{RTG} - T_{E,D}) - \epsilon_{E,D} \cdot \sigma_b \cdot S_{E,D} \cdot T_{E,D}^4] \tag{5.12}$$

Distribution Node 2:

$$0 = 4 \cdot [CON_{10} \cdot (T_{Node_1} - T_{Node_2}) + CON_{11} \cdot (T_{E,D} - T_{Node_2}) +$$

$$+ CON_{13} \cdot (T_{Ground} - T_{Node_2})] \tag{5.13}$$

E.2 Heat conductance

Table E.3: Definition of heat conductance C between the nodes according to Figure 4.9.

Name	Linked Components	Geometry
Linkage	**RTG $\leftrightarrow$ Chassis**	

$CON_2 = CON_I + n_B \cdot CON_B$

$CON_2 = 1.50 \cdot 10^{-1} \; \frac{W}{K}$

Part	Cross section	Thickness	Material	Amount
Insulation	$A_I = 3'770 mm^2$	$t_I = 12 mm$	Aerogel	1
Bolts, M6	$A_B = 28.3 mm^2$	$t_B = 12 mm$	Titan	10
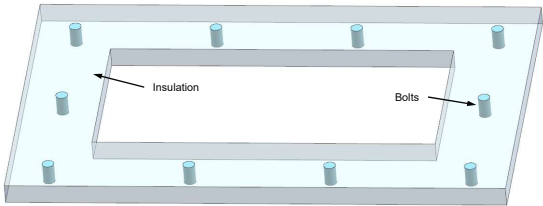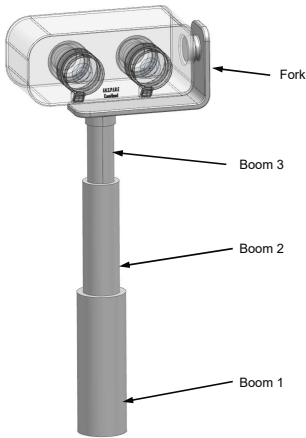
Name	Linked Components	Geometry
Linkage	**EBay $\leftrightarrow$ Chassis**	

$CON_3 = CON_I + n_B \cdot CON_B$

$CON_3 = 2.80 \cdot 10^{-1} \; \frac{W}{K}$

Part	Cross section	Thickness	Material	Amount
Insulation	$A_I = 27'120 mm^2$	$t_I = 12 mm$	Aerogel	1
Bolts, M6	$A_B = 28.3 mm^2$	$t_B = 12 mm$	Titan	10

Table E.4: Definition of heat conductance $C = \frac{1}{R}$ between the nodes according to Figure 4.9.

Name	Linked Components	Geometry
Telescope	**Camera $\leftrightarrow$ Chassis**	

$$CON_6 = \left(\frac{1}{CON_{B1}} + \frac{1}{CON_{B2}} + \frac{1}{CON_{B3}} + \frac{1}{CON_F} \right)^{-1}$$

$$CON_6 = 7.10 \cdot 10^{-2} \, \frac{W}{K}$$

Part	Cross section	Thickness	Material	Amount
Boom 1	$A_{B1} = 181mm^2$	$t_{B1} = 116mm$	Aluminium	1
Boom 2	$A_{B2} = 134mm^2$	$t_{B2} = 95mm$	Aluminium	1
Boom 3	$A_{B3} = 97mm^2$	$t_{B3} = 60mm$	Aluminium	1
Fork	$A_F = 200mm^2$	$t_F = 170mm$	Aluminium	1
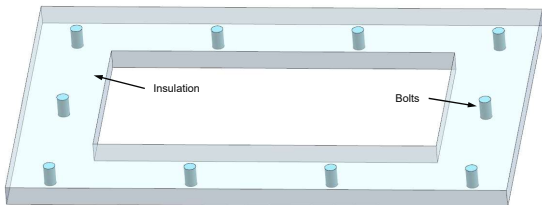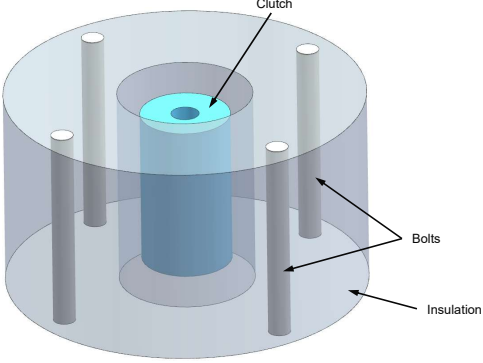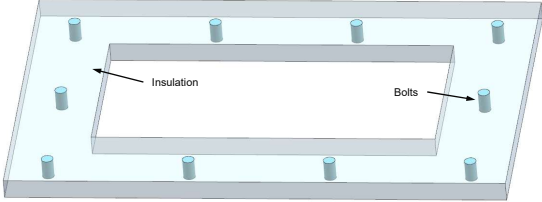
Name	Linked Components	Geometry
Suspension	**Node$_1$ $\leftrightarrow$ Chassis**	

$$CON_7 = 1.61 \cdot 10^{-1} \, \frac{W}{K}$$

Part	Cross section	Thickness	Material	Amount
Suspension	$A_S = 137mm^2$	$t_S = 201mm$	Aluminium	1

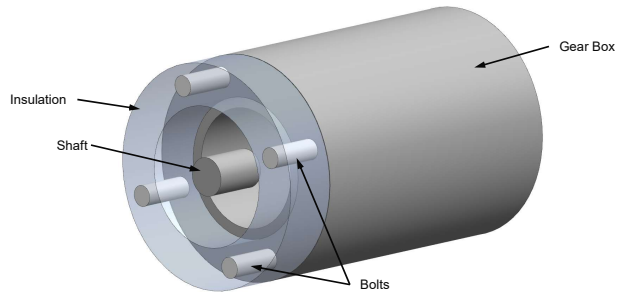Table E.5: Definition of heat conductance $C = \frac{1}{R}$ between the nodes according to Figure 4.9.

Name	Linked Components	Geometry
Mounting	**Steer Engine $\leftrightarrow$ Node$_1$**	

$$CON_8 = CON_C + CON_I + n_B \cdot CON_B$$

$$CON_8 = 6.85 \cdot 10^{-1} \; \frac{W}{K}$$

Part	Cross section	Thickness	Material	Amount
Clutch	$A_C = 45.4 mm^2$	$t_C = 14mm$	Aluminium	1
Insulation	$A_I = 691 mm^2$	$t_I = 18mm$	Aerogel	1
Bolts	$A_B = 3.14 mm^2$	$t_B = 18mm$	Steel	4
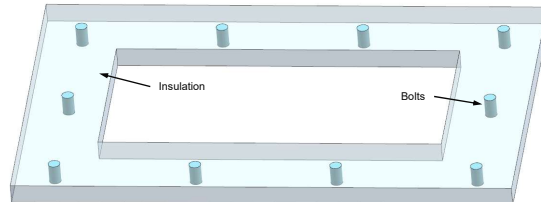
Name	Linked Components	Geometry
Wheel Fork	**Node$_1$ $\leftrightarrow$ Node$_2$**	

$$CON_{10} = 2.29 \cdot 10^{-1} \; \frac{W}{K}$$

Part	Cross section	Thickness	Material	Amount
Wheel Fork	$A_{WF} = 200 mm^2$	$t_{WF} = 175$	Aluminium	1

Table E.6: Definition of heat conductance $C = \frac{1}{R}$ between the nodes according to Figure 4.9.

Name	Linked Components	Geometry
Mounting	**Drive Engine $\leftrightarrow$ Node$_2$**	

$$CON_{11} = \left(\frac{1}{CON_G} + \frac{1}{CON_S + CON_I + n_B \cdot CON_B} \right)^{-1}$$

$$CON_{11} = 2.19 \cdot 10^{-1} \frac{W}{K}$$

Part	Cross section	Thickness	Material	Amount
Gear Box	$A_G = 566mm^2$	$t_G = 43.1mm$	Steel	1
Shaft	$A_S = 23.8mm^2$	$t_S = 8mm$	Steel	1
Insulation	$A_I = 490mm^2$	$t_I = 8mm$	Aerogel	1
Bolts, M3	$A_B = 7.07mm^2$	$t_B = 8mm$	Steel	4

Name	Linked Components	Geometry
Rim	**Node$_2$ $\leftrightarrow$ Ground**	

$$CON_{13} = 5.11 \cdot 10^{-3} \frac{W}{K}$$

Part	Cross section	Thickness	Material	Amount
Rim	$A_R = 12mm^2$	$t_r = 100mm$	Titan	6

Note: It was assumed, that the wheel temperature equals the ground temperature because of the remarkable difference of the heat conduction, $\frac{\lambda_{Wheel}}{\lambda_{Rim}} = 28.2$.

E.3 Heat switch

The charateristic of the switch conductance depends on the mean temperature T_M, shown by measurements in cite . As this temperature won´t be calculated in the analysis, the corresponding component temperature T_C shall be used. In order to describe the characteristic, it was divided in three sections, Figure E.10. The temperature where the disk decouples is $T_{toggle} = 108K$ and not applicable for the current application. By reducing the heigt, the toggle temperature can be increased and the characteristic can be shifted to higher termperatures ("'to the right"'). It was assumed, that the gradients of section 2 and 3 as well as the temperature range of section 2 keep constant. The axis interseption is a function the toggle temperature $(a_2 = f(\Delta T_{toggle})$, $\Delta T_{Toggle} = T_{new} - T_{old}|_{toggle})$.

Table E.7: Sections and range of the switch characteristic.

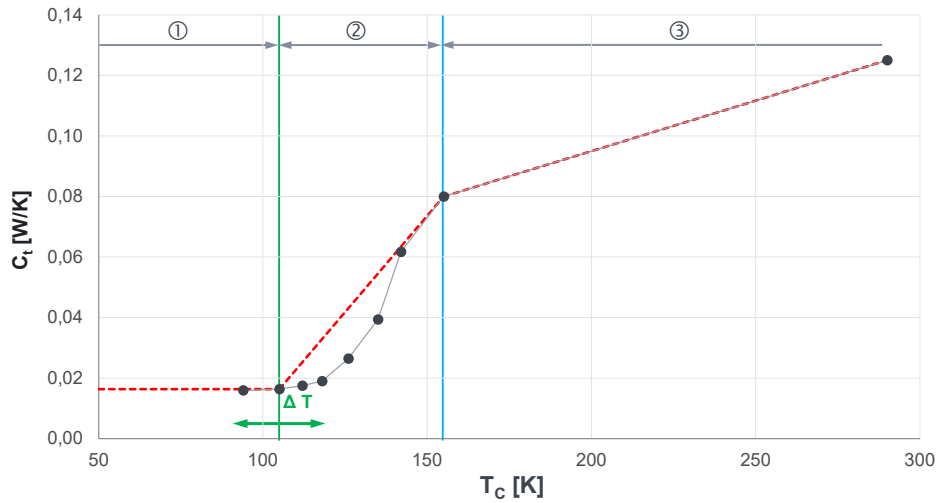| Section	Temperature range	Hear conductance $C_t = \frac{1}{R_t}$
1	$T_{toggle} > \quad T_C$	$C_{t,1} = 16.4 \cdot 10^{-3} \frac{W}{m^2 K} = const.$
2	$T_{toggle} \leq \quad T_C \quad < T_1$	$C_{t,2}(T_C) = a_{1.1} \cdot T_C + a_{1.2}$
		$a_{1.1} = +1.272 \cdot 10^{-3} \frac{W}{m^2 K^2}$
		$a_{1.2} = -1.272 \cdot 10^{-3} \frac{W}{m^2 K^2} \cdot \Delta T_{Toggle} - 0.117 \frac{W}{m^2 K}$
3	$T_C \quad > T_1$	$C_{t,3}(T_C) = a_{2.1} \cdot T_C + a_{2.2}$
		$a_{2.1} = +333 \cdot 10^{-6} \frac{W}{m^2 K^2}$
		$a_{2.2} = -333 \cdot 10^{-6} \frac{W}{m^2 K^2} \cdot \Delta T_{Toggle} - 28.3 \cdot 10^{-3} \frac{W}{m^2 K}$

Figure E.10: Conductance characteristic of heat switch diveded in sections.

E.4 Rover absorptivity

The amount of solar radiation onto the rover depends on the sun altitude, see autoref(fig:tcsabsop).

View Factor 1, Inclination: $\quad \varphi_1 = \cos(\lambda) \cdot \cos(\delta)$

View Factor 2, Declination: $\quad \varphi_2 = \cos(90° - \lambda) \cdot \cos(\delta)$

E.5 Values

Table E.8: Temperatur limits of the rover components.

	Temperature limits in [$°C$]	
Component	min.	max.
Command & Data Handling		
Transmitter	-10	50
Receiver	-30	70
PCDU	-40	60
Battery	-35	60
Camera	-40	70
Objektive	-40	71
Steering Engine	-30	100
Drive Engine	-40	100
Drive Gear	-40	100

The Europa ground temperature varies at the equator between $T_{e,min} = 80K$ and $T_{e,max} = 130K$, depending on the sun inclination. The temperature at the pole is $T_{Pole} = 50K$, cite(europa). It was assumed, that the ground temperature depends on the sun altitude. A trigonometrical interpolation was defined as follows.

$$T_{Ground}(\lambda,\delta) = T_{Pole} + \cos(\delta) \cdot [(T_{e,min} + \cos(\lambda) \cdot (T_{e,max} - T_{e,min})) - T_{Pole}]$$

For λ and δ see Subsection E.4.

Table E.9: Minimum and maximum of surface emisivity and absorptivity values.

	Emisivity [-]		Absorptivity [-]		Source
Surface finishing	min.	max.	min.	max.	
Aluminium, polished		0.05		0.2	
Aluminium, sand blasted		0.2		0.4	
White paint	0.8	0.9	0.2	0.5	

Table E.10: Heat conductivity in $\frac{W}{mK}$

Material	Nominal	Used	Source
Aerogel	0.002 - 0.05	0.05	[18]
Aluminium[1]	110 - 240	200	
Steel[1]	21 - 50	50	
Titan[1]	7.1	7.1	

[1] depends on the alloying component, a conservative value was choosen

Table E.11: Radiation surface and finishing of components.

Part	Surface m^2	Finishing	Note
Chassis - top/bottom	$A_{Chas,tb} = 0.086$		for albedo
Chassis - side	$A_{Chas,s} = 0.085$		for albedo
Chassis - total	$A_{Chas,t} = 0.388$		for emisivity
Camera - housing	$A_{Cam,h} = 0.011$		
Camera - radiator	$A_{Cam,rad} = 0.???$	white paint	
Steer Engine	$A_{E,S} = 0.1$		
Drive Engine	$A_{E,D} = 0.04$		
Electric Bay	$A_{Bay} = 0.146$	aluminium, sand blastet	
RTG	$A_{RTG} = 0.086$	white paint	